X-ray crystal structure and theoretical analysis of Au 25- xAgx(SCH2CH2Ph) 18- alloy

ARTICLE *in* JOURNAL OF PHYSICAL CHEMISTRY LETTERS · FEBRUARY 2014

Impact Factor: 7.46 · DOI: 10.1021/jz402441d

3 AUTHORS, INCLUDING:

Amala Dass
University of Mississippi
108 PUBLICATIONS **3,287** CITATIONS
SEE PROFILE

Chanaka Kumara
University of Mississippi
20 PUBLICATIONS **307** CITATIONS
SEE PROFILE

THE JOURNAL OF PHYSICAL CHEMISTRY Letters

Letter

pubs.acs.org/JPCL

X-ray Crystal Structure and Theoretical Analysis of $Au_{25-x}Ag_x(SCH_2CH_2Ph)_{18}^-$ Alloy

Chanaka Kumara,[†] Christine M. Aikens,[§] and Amala Dass*[,†]

[†]Department of Chemistry and Biochemistry, University of Mississippi, Oxford, Mississippi 38677, United States

[§]Department of Chemistry, Kansas State University, Manhattan, Kansas 66506, United States

Supporting Information

ABSTRACT: The atomic arrangement of Au and Ag atoms in $Au_{25-x}Ag_x(SR)_{18}$ was determined by X-ray crystallography. Ag atoms were selectively incorporated in the 12 vertices of the icosahedral core. The central atom and the metal atoms in the six [−SR−Au−SR−Au−SR−] units were exclusively gold, with 100% Au occupancy. The composition of the crystals determined by X-ray crystallography was $Au_{18.3}Ag_{6.7}(SCH_2CH_2Ph)_{18}$. This composition is in reasonable agreement with the composition $Au_{18.8}Ag_{6.2}(SCH_2CH_2Ph)_{18}$ measured by electrospray mass spectrometry. The structure can be described in terms of shells as $Au_1@Au_{5.3}Ag_{6.7}@6\times[-SR-Au-SR-Au-SR-]$. Density functional theory calculations show that the electronic structure and optical absorption spectra are sensitive to the silver atom arrangement within the nanocluster.

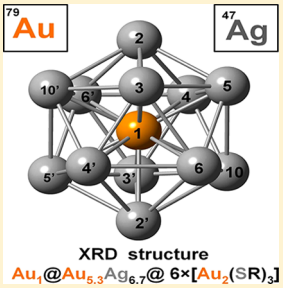

SECTION: Physical Processes in Nanomaterials and Nanostructures

Among the various Au_nSR_m molecules, $Au_{25}(SR)_{18}$ is the most commonly studied due to its interesting optical[1] and electrochemical[2] properties and high stability. In the $Au_{25}(SR)_{18}$ family of molecules, several alloys have been synthesized by different research groups including $Au_{25-x}Ag_x(SR)_{18}^-$ (ref 3), $Au_{24}Pd(SR)_{18}$ (ref 4), $Au_{25-x}Cu_x(SR)_{18}$ (ref 5), and $Au_{24}Pt(SR)_{18}$ (ref 6). The central atom of the 13-atom icosahedral core can be replaced by Pd in both thiols and phosphine[7] protected ultrasmall gold nanoparticles. Among these reports, Ag atom doping exhibits maximum heteroatom incorporation, which is up to 12 silver atoms. Similar atomic radii, lattice parameters, and electronic properties between Au and Ag facilitate this interesting maximum atom incorporation. Walter et al.[8] and Guidez et al.[9] show that silver incorporation in the center of the core is not energetically favorable compared to other possible locations; the surface of the icosahedral core is energetically preferred. Other reports[10] also predict similar results.

In terms of Ag doping on other Au_nSR_m molecules, we recently reported the synthesis, isolation, and optical properties of ultrasmall $Au_{38-x}Ag_x(SR)_{24}$ and $Au_{144-x}Ag_x(SR)_{60}$ alloys of Au-SR molecules.[11,12] In the case of $Au_{38-x}Ag_x(SR)_{24}$, the silver atoms are predicted to be in the surface of the central core. Computational studies show that Ag atoms incorporated into the 60-atom rhombicosidodecahedron shell[13,14] of the Au_{144} model are the most energetically favored ones.[15] While these predictions based on theoretical/computational calculations exist, there is a lack of experimental evidence for the location of the doped atoms. Crystal structures of the $Au_{25}(SR)_{18}$ molecule were reported by the Murray and Jin groups.[16,17] Crystal structures of the $Ag_{44}(SR)_{24}$ nanomolecule[18,19] and its Au alloy,[19] $Ag_{32}Au_{12}(SR)_{24}$, and other metal alloys[13,14] were also reported recently. However, the surface metal−sulfur interfacial structure of these silver-based alloy nanoparticles differs from that of the gold-based alloy nanoparticles. Therefore, the crystal structures of Ag_{44} alloys do not aid in the experimental identification of silver sites in our system. Currently, there is a void in our understanding of the location of Ag atoms in Au-SR molecules due to the lack of crystal structure investigations of Ag-doped Au-SR alloy molecules.

Herein, we report the experimentally determined locations of silver atoms in the $Au_{25-x}Ag_x(SCH_2CH_2Ph)_{18}^-$ structure based on X-ray crystallography. To our knowledge, this is the first X-ray crystal structure of alloys of Au-SR molecules. The $Au_{25-x}Ag_x(SCH_2CH_2Ph)_{18}^-$ molecules were synthesized using a modified procedure reported by Negishi.[3] Briefly, the synthesis involves two steps. The first step is the synthesis of a crude product that contains polydisperse Au−Ag clusters. The second step is solvent fractionation to isolate $Au_{25-x}Ag_x(SCH_2CH_2Ph)_{18}^-$ molecules. (See the Experimental Section for details.) Figure 1 shows the crystal structure of $Au_{25-x}Ag_x(SCH_2CH_2Ph)_{18}^-$, which crystallizes in a triclinic $P\bar{1}$. The structure was refined to a resolution of 0.8 Å and to an R_1 value of 4.1%. There are three different distinct locations where the metal atom can be doped into the $Au_{25}(SR)_{18}$ structure, (1) the single central atom of the icosahedral core, (2) the 12 atoms in the vertices of the icosahedral core, and (3) the 12 Au atoms forming the six dimeric [−SR−Au−SR−Au−SR−] units.

Figure 1 shows the X-ray crystallographic structure of $Au_{25-x}Ag_x(SCH_2CH_2Ph)_{18}^-$. Specifically, the crystals considered in this study have the composition $Au_{18.3}Ag_{6.7}(SCH_2CH_2Ph)_{18}^-$. The central atom was shown to

Received: November 12, 2013
Accepted: January 5, 2014
Published: January 17, 2014

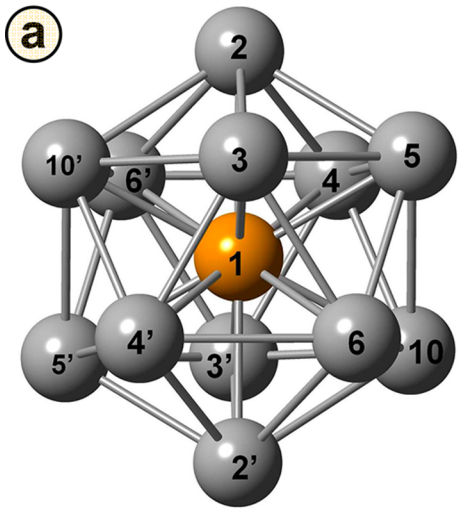

Sites	Ag %	Au %	Total Ag	Total Au
1	0	100	0	1
2, 2'	59	41	1.18	0.82
3, 3'	45	55	0.90	1.10
4, 4'	61	39	1.21	0.78
5, 5'	58	42	1.16	0.84
6, 6'	53	47	1.06	0.96
10, 10'	56	44	1.12	0.88
(S-Au-S-Au-S) x 6	0	100	0	12
Total metal atoms			6.7	18.3
Composition from crystal structure	$Au_{18.3}Ag_{6.7}(SR)_{18}$			
Composition from mass spectrometry	$Au_{18.8}Ag_{6.2}(SR)_{18}$			

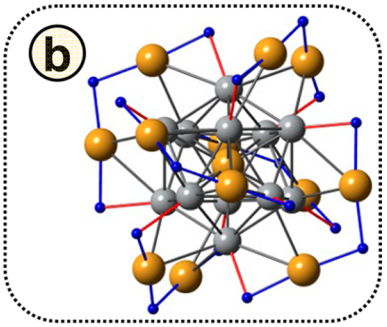

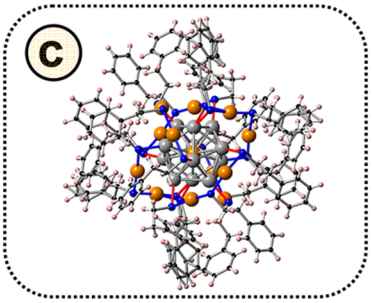

Au_1 @ $Au_{5.3}Ag_{6.7}$ @ 6×[-SR-Au-SR-Au-SR-]

Figure 1. X-ray crystal structure of the $Au_{25-x}Ag_x(SCH_2CH_2Ph)_{18}$ anion. The X-ray crystallography-based composition is $Au_{18.3}Ag_{6.7}(SCH_2CH_2Ph)_{18}^-$. This can be written as $Au_1@Ag_{5.3}Au_{6.7}@6\times[-SR-Au-SR-Au-SR-]$ (a) The 13-atom icosahedral alloy core geometry, showing a central Au atom (yellow) with 100% Au occupancy surrounded by 12 atoms that show partial occupancy of Au or Ag atoms, as shown in the inset table (B) $Au_{25}S_{18}$ framework showing the six [−SR−Au−SR−Au−SR−] dimeric units, where the dimeric units exclusively contain Au atoms, with 100% Au occupancy. (c) Total structure of $Au_{25-x}Ag_x(SCH_2CH_2Ph)_{18}^-$. Blue lines indicate Au−S bonds; red lines indicate possible Ag−S or Au−S bonds; yellow is Au, gray is Ag or Au, and blue is S. (see table B) The inset table and (a) show that the 12 atoms at the icosahedral vertices are partially occupied by Ag or Au. The X-ray crystallographic structure is an *average* structure; that is, the X-ray composition $Au_{18.3}Ag_{6.7}(SCH_2CH_2Ph)_{18}^-$ is the average value obtained from diffraction of many $Au_{25-x}Ag_x(SR)_{18}$ molecules in the crystal. The structure in (a) is an average structure denoting that among the many $Au_{25}(SR)_{18}$ molecules that diffracted, the Ag atoms were found distributed among the 12 icosahedral vertex atoms, with slight preference for sites 2, 2′, 4, 4′, 5, 5′, 10, and 10′ when compared with 3, 3′, 6, and 6′. For any individual $Au_{25}(SR)_{18}$ molecule in the crystal, however, the composition is likely to be $Au_{21}Ag_4(SR)_{18}$, $Au_{20}Ag_5(SR)_{18}$, $Au_{19}Ag_6(SR)_{18}$, $Au_{18}Ag_7(SR)_{18}$, and $Au_{17}Ag_8(SR)_{18}$ with probabilities of 3.3, 19.4, 42.3, 28.8, and 6.6%, respectively, as shown by ESI-MS spectra in Figure 2. The composition obtained independently by ESI-MS is $Au_{18.8}Ag_{6.2}(SCH_2CH_2Ph)_{18}$, in reasonable agreement with X-ray crystallographic composition. See the text, ESI-MS data, and Table 1 for further details and discussions.

be exclusively Au (occupancy factor = 1.00), as predicted.[9] The 12 atoms in the vertices of the icosahedral $Au_{12-x}Ag_x$ core show dual occupancy, containing either Au atoms or Ag atoms, as shown in Figure 1a. The overall composition of the $metal_{13}$ core from X-ray crystallography is $Au_1@Au_{5.3}Ag_{6.7}$. The composition was independently verified using mass spectrometry. The compositional disorder of Au and Ag atoms yielded fractional occupancies. For example, location 2 is occupied by either atoms Ag2 or Au2, with the Ag2 atom being present 59% of the time. This is denoted as Ag2/Au2 = 59/41%. Figure 1a (inset table) shows the following percentages of Ag or Au atoms: Ag3/Au3 = 45/55%, Ag4/Au4 = 61/39%, Ag5/Au5 = 58/42%, Ag6/Au6 = 53/47%, and Ag10/Au10 = 56/44%. Therefore, the metal core composition can be formulated as $Au_{5.3}Ag_{6.7}$. The metal atoms in the dimeric staple groups contain exclusively gold, with 100% Au occupancy.

The dopant positions of silver atom in the 13-atom icosahedral core of Au_{25} have been computationally predicted before but have not been determined experimentally until now. It is interesting to note that the greatest (4 and 4′ site) and least Ag (3 and 3′ site) occupancy sites are located on the same plane (Figure S3, Supporting Information). We observed partially occupied counterions and solvent molecules (see the Supporting Information). There is clear evidence for the presence of the tetraoctylammonium counterion, but it was not modeled in this work. It is very likely that the counterions and solvent molecules are disordered over several positions. This may be due to solvent loss or a disordered solvent channel that increases the mosaicity of the crystals, hindering the identification of the exact location of the counterions. The upper limit of the volume that can be occupied by the solvent was calculated to be 9592 $Å^3$, or 19.9% of the unit cell volume.

When compared with the monometallic $Au_{25}(SCH_2CH_2Ph)_{18}^-$ crystal structures,[16,17] we observed that the major structural features (the $metal_{13}$ icosahedral core protected by six [−SR−Au−SR−Au−SR−Au−] units) are preserved upon silver doping. The silver atoms are simply substituted among the 12 vertices of the icosahedron core. In general, bond elongations were observed from the central Au atom to icosahedral surface atoms as the Ag content increased (Figure S4, Supporting Information).

The mass spectrum shows that the crystals are actually a mixture of $Au_{21}Ag_4(SR)_{18}$, $Au_{20}Ag_5(SR)_{18}$, $Au_{19}Ag_6(SR)_{18}$, $Au_{18}Ag_7(SR)_{18}$, and $Au_{17}Ag_8(SR)_{18}$. From the peak height of each species, the average composition of the crystal was found to be $Au_{18.8}Ag_{6.2}(SCH_2CH_2Ph)_{18}$. The inset shows the mass spectrum of the crystal showing peaks for only

dx.doi.org/10.1021/jz402441d | J. Phys. Chem. Lett. 2014, 5, 461−466

$Au_{25-x}Ag_x(SR)_{18}$. See Table 1 and the text for further discussion.

Table 1. Average Composition Determined by Mass Spectrometry Data

nanomolecules	% Ag as total[a]	contribution of silver from each species
$Au_{21}Ag_4(SR)_{18}$	3.3	0.13
$Au_{20}Ag_5(SR)_{18}$	19.4	0.97
$Au_{19}Ag_6(SR)_{18}$	42.3	2.54
$Au_{18}Ag_7(SR)_{18}$	28.8	2.02
$Au_{17}Ag_8(SR)_{18}$	6.1	0.49
total number of Ag from ESI-MS		6.15 ≈ 6.2

[a]Taken from mass spectrometry data.

Crystals of the title nanomolecules were analyzed using electrospray mass spectrometry (ESI-MS). This will faciliate the determination of the composition that is complementary to but independent of X-ray crystallographic composition. Figure 2

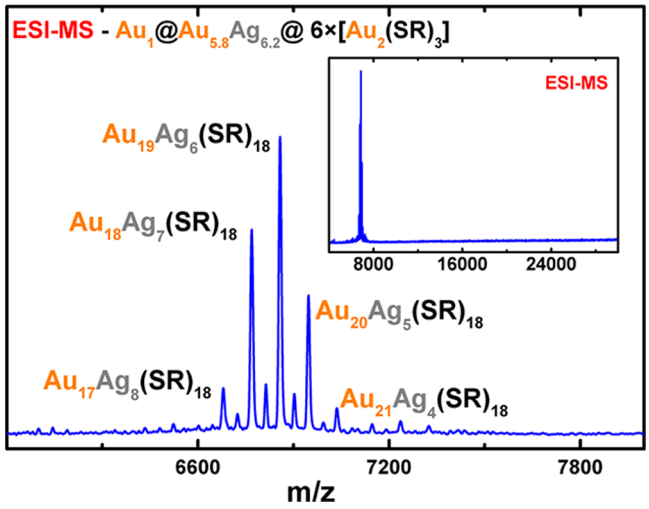

Figure 2. Electrospray mass spectrum (ESI-MS) of the $Au_{25-x}Ag_x(SCH_2CH_2Ph)_{18}^-$ crystals.

shows the ESI mass spectrum, containing peaks corresponding to $Au_{17}Ag_8(SR)_{18}$, $Au_{18}Ag_7(SR)_{18}$, $Au_{19}Ag_6(SR)_{18}$, $Au_{20}Ag_5(SR)_{18}$, and $Au_{21}Ag_4(SR)_{18}$ nanomolecules, present in 0.061, 0.288, 0.423, 0.194, and 0.033 fractions, respectively.[20] Then, the percentages of each of these species were calculated from the peak height corresponding to each species in the ESI-MS spectrum, as shown in Table 1. Finally, using these percentages, the average composition was calculated and found to be $Au_{18.8}Ag_{6.2}(SR)_{18}$. This can be written as $Au_1@Ag_{6.2}Au_{5.8}@6\times[-SR-Au-SR-Au-SR-]$.

X-ray crystallography also yields the average structure and average composition, which is independently derived as 6.7 silver atoms, with the composition $Au_{18.3}Ag_{6.7}(SCH_2CH_2Ph)_{18}$. Therefore, mass spectrometry and X-ray crystallography show 6.2 and 6.7 Ag atoms, respectively. This is a reasonable agreement, and the differences may be due to the fact that the ESI peak heights are correlated to ionization efficiencies and may slightly differ from what is present in solution.

UV−visible spectra show that the features change upon silver atom doping. These features are further investigated using theoretical calculations. However, due to configurational disorder, the experimental optical absorption spectrum is expected to be a Boltzmann average of the spectra of several structures. We have chosen to examine two low-energy structures for careful analysis.

For the theoretical calculations, one structure (isomer **1**) is constructed in which atoms 2, 2′, 4, 4′, 5, and 5′ are chosen to be silver atoms because these positions have the highest silver content in the crystal structure. This leads to a structure in which three silver atoms on each side of the icosahedral core are separated by a ring of gold atoms, as shown in Figure 3.

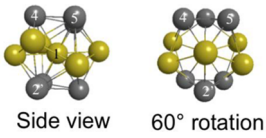

Figure 3. Silver atom arrangement in the core of $Au_{19}Ag_6(SCH_2CH_2Ph)_{18}^-$ structure **1**. The silver atom arrangement in structure **2** has an identical pattern. The six [−SR−Au−SR−Au−SR−] units are omitted for clarity.

Bond distances are maintained at the average crystal structure distances regardless of which metal atom actually occupies the site; the crystal structure distances represent an average due to the configurational disorder in the crystal. It should be noted that the positions with greater average silver content generally have the longest average bond distances from Au1. This lengthening of the Au−Ag bond was previously predicted theoretically.[9] A second structure (**2**) is also constructed in which atoms 4, 4′, 5, 5′, 10, and 10′ are chosen to be silver atoms because these positions have the first, third, and fourth greatest amount of silver content and this structure also has three silver atoms on each side of the icosahedral core separated by a ring of six gold atoms, which is identical to the pattern shown in Figure 3 for structure **1**. These isomers are similar to the 6d $Au_{19}Ag_6(SH)_{18}^-$ structure in ref 9 examined previously.[9] The calculations presented in this work employ the coordinates of the full phenylethanethiolate ligands as determined from the crystal structure. The coordinates were not reoptimized. The electronic structure of the pure $Au_{25}(SCH_2CH_2Ph)_{18}^-$ nanoparticle has been previously discussed.[17]

Structure **1** is predicted to lie 0.01 eV lower in energy than **2** at the LB94/DZ level of theory. For both **1** and **2**, the HOMO of the system is the P superatomic orbital that points toward the two sets of three silver atoms (Figure 4). In **1**, this orbital lies 0.29 eV higher in energy above the next P orbital, and the lowest P orbital lies a further 0.26 eV lower in energy (Figure S6, Supporting Information). For **2**, the two lower-energy P orbitals are nearly degenerate and are split by only 0.03 eV; they lie 0.36 eV below the HOMO. In **2**, the HOMO is directed toward the areas of the nanoparticle with low ligand density. The perpendicular HOMO−1 and HOMO−2 P orbitals are oriented toward portions of the nanoparticle with a higher ligand density; they are in similar environments, and therefore, it is not surprising that they are found to be nearly degenerate. In contrast, the HOMO of **1** is not pointed toward the low ligand density part of the nanoparticle, and the two perpendicular P orbitals have somewhat different environments. The LUMO and LUMO+1 of both **1** and **2** have D-like character. These two low-energy D orbitals do not form a degenerate set; they are split by 0.25 (**1**) and 0.09 eV (**2**). Unlike $Au_{25}(SH)_{18}^-$ and $Ag_{25}(SH)_{18}^-$,[21] the other three

dx.doi.org/10.1021/jz402441d | J. Phys. Chem. Lett. 2014, 5, 461−466

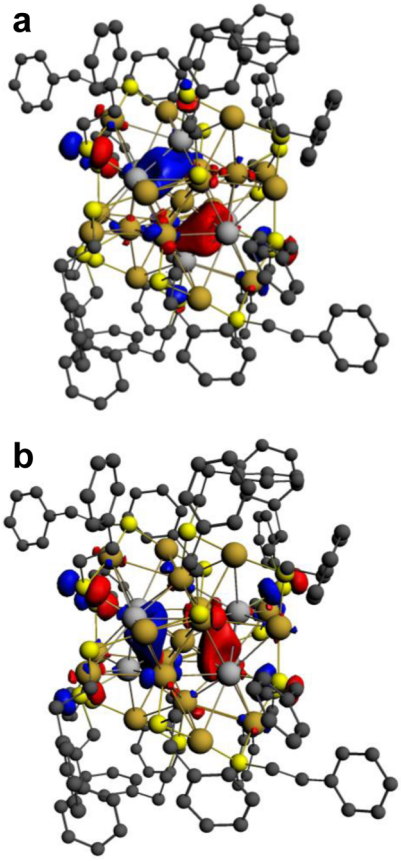

Figure 4. HOMO P orbitals of (a) structure **1** and (b) structure **2**.

superatomic D orbitals do not lie directly above the first two. Instead, π^* orbitals from the phenyl groups are predicted to form the LUMO+2 and higher orbitals; some D character is mixed into a few of these orbitals including the LUMO+6.

The TDDFT optical absorption spectra of **1** and **2** are shown in Figure 5. The first two peaks for each (740−900 nm) arise from transitions from the HOMO into the LUMO and LUMO +1. This tail is similar to that exhibited in the experimental UV−vis spectrum for the mixed $Au_{25-x}Ag_x(SCH_2CH_2Ph)_{18}^-$ molecules. Transitions from the other two P orbitals

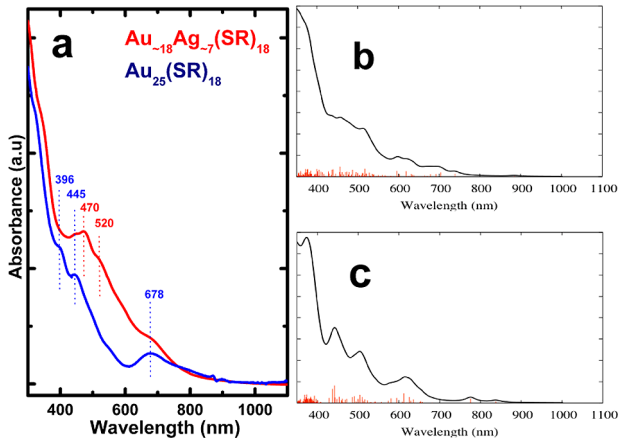

Figure 5. (a) Experimental UV−vis−NIR spectra of $Au_{25}(SCH_2CH_2Ph)_{18}^-$ (blue) in comparison with $Au_{25-x}Ag_x(SCH_2CH_2Ph)_{18}^-$ alloy (red) in toluene. (b,c) Theoretical absorption spectra of structures **1** and **2**.

(HOMO−1 and HOMO−2) into the LUMO and LUMO+1 fall around 620−700 nm for **1** and 650−700 nm for **2**. For **1** and **2**, transitions into the π^* orbitals are predicted to become important at around 690 nm. Both **1** and **2** exhibit structures in the 400−650 nm region that are similar to those in the experimental UV−vis spectrum.

In summary, the crystal structure of $Au_{25-x}Ag_x(SCH_2CH_2Ph)_{18}^-$ is presented, which is the first X-ray crystallography report of a $Au_{25}(SR)_{18}$ alloy family. We show that the central atom is exclusively Au with 100% occupancy, while the 12-atom icosahedral vertex atoms are partially occupied by Ag or Au atoms. The six staples are exclusively occupied by Au, with the [−SR−Au−SR−Au−SR−] structure. Ag incorporation shows a site-specific distribution in the $Au_{25}(SR)_{18}$ structure leading to a Au−(Au/Ag)−Au heterometal atom configuration, more specifically the $Au_1@Au_{5.3}Ag_{6.7}@6\times$[−SR−Au−SR−Au−SR−] arrangement. Overall, the incorporation of silver atoms into a gold nanoparticle has significant effects on the electronic structure and optical absorption spectrum. Silver affects the orientation of the HOMO orbital. The effects of silver on the electronic structure are noticeable even for two structures with relatively similar silver arrangement.

EXPERIMENTAL SECTION

Synthesis of $Au_{25-x}Ag_x(SCH_2CH_2Ph)_{18}^-$. The $Au_{25-x}Ag_x(SCH_2CH_2Ph)_{18}^-$ were synthesized via the previously reported procedure by Negishi[3] in two steps. An aqueous solution (30 mL) containing $HAuCl_4$ and $AgNO_3$ (the total metal concentration was set to 30 mM) was mixed with a toluene solution (30 mL) of tetraoctylammonium bromide, TOABr (1.1 mmol). The initial mole ratios of Au/Ag precursors were varied up to 1:0.66. After stirring for 30 min, the turbid organic phase was separated, and phenylethane thiol (10 mmol) was added and further stirred for 30 min at room temperature. This solution was cooled in an ice bath for 30 min. An aqueous solution of $NaBH_4$ (20 mmol, 20 mL) cooled to 0 °C was rapidly added to the reaction mixture under vigorous stirring. After 3 h, the organic layer was separated and evaporated to dryness. The product was washed with methanol to remove excess thiol, $NaBH_4$, TOABr, and other byproducts. The residual mixture was extracted with CH_3CN.

The product mixture was dissolved in toluene, and then, solvent fractionation was performed using CH_3CN to isolate $Au_{25-x}Ag_x(SCH_2CH_2Ph)_{18}^-$. Several crystallization setups were conducted using toluene or CH_2Cl_2 as a solvent and EtOH or MeOH as a nonsolvent. The crystallization setups with higher Au/Ag ratios either decomposed or precipitated without forming crystals. However, crystals were found in dried form in the Au/Ag 1:0.25 incoming molar ratio synthesis. This batch of crystals was used for X-ray crystallography.

Characterizations. UV−visible spectra were obtained in toluene solutions using a Shimadzu UV-1601 spectrometer in the 300−1100 nm range, and the analysis was performed using Shimadzu UVProbe 2.0 software. ESI mass spectra were obtained from a Waters SYNAPT mass spectrometer in a 50:50 toluene/CH_3CN solvent mixture or THF.

Computational Details. Coordinates for isomers **1** and **2** were obtained from the experimental crystal structure, as described above. Time-dependent density functional theory (TD-DFT) computations were performed using the LB94[22] exchange−correlation potential. A double-ζ basis set of Slater orbitals with a 1s frozen core for C, a 4p frozen core for Ag, and a 4f frozen

dx.doi.org/10.1021/jz402441d | J. Phys. Chem. Lett. 2014, 5, 461−466

core for Au was employed in the calculations. The zeroth-order regular approximation (ZORA)[23] was employed to account for scalar relativistic effects. Five hundred excited states were determined, which corresponds to excitation energies up to 4.1 eV. The Amsterdam Density Functional (ADF) program[24] was employed for all calculations. Orbitals were plotted with a contour value of 0.03.

Single Crystal X-ray Analysis. A black crystal with approximate dimensions of 0.08 × 0.07 × 0.02 mm^3 was selected under oil under ambient conditions and attached to the tip of a MiTeGen MicroMount. The crystal was mounted in a stream of cold nitrogen at 100(1) K and centered in the X-ray beam by using a video camera. The crystal evaluation and data collection were performed on a Bruker Quazar SMART APEXII diffractometer with Mo K_α (λ = 0.71073 Å) radiation and the diffractometer to crystal distance of 4.96 cm. The initial cell constants were obtained from three series of ω scans at different starting angles. Each series consisted of 12 frames collected at intervals of 0.5° in a 6° range about ω with the exposure time of 20 s per frame. The reflections were successfully indexed by an automated indexing routine built in the APEXII program suite. The final cell constants were calculated from a set of 9092 strong reflections from the actual data collection. The data were collected by using the full sphere data collection routine to survey the reciprocal space to the extent of a full sphere to a resolution of 0.80 Å. A total of 58305 data were harvested by collecting 4 sets of frames with 0.5° scans in ω and φ with exposure times of 40 s per frame.

Crystal data for $C_{144}H_{162}Ag_{6.6587}Au_{18.3413}S_{18}$ (M = 6800.70): triclinic, space group P-1 (no. 2), a = 16.191(7) Å, b = 17.244(7) Å, c = 18.613(7) Å, α = 105.871(12)°, β = 106.252(13)°, γ = 90.74(2)°, V = 4776(3) $Å^3$, Z = 1, T = 100.01 K, μ(Mo K_α) = 14.917 mm^{-1}, D_{calc} = 2.364 g/mm^3, 58305 reflections measured (2.38 ≤ 2Θ ≤ 56.718), 23796 unique (R_{int} = 0.0426), which were used in all calculations. The final R_1 was 0.0411 ($I > 2\sigma(I)$), and wR_2 was 0.1065 (all data).

■ ASSOCIATED CONTENT

Supporting Information

Mass spectrometric data, supplementary crystallographic data, electronic energy levels of 1,2 and .cif file. CCDC reference number is 973795. This material is available free of charge via the Internet at http://pubs.acs.org.

■ AUTHOR INFORMATION

Corresponding Author

*E-mail: amal@olemiss.edu.

Notes

The authors declare no competing financial interest.

■ ACKNOWLEDGMENTS

C.K. and A.D. gratefully acknowledge support from NSF CHE-1255519 and the University of Mississippi Startup Fund. C.M.A. gratefully acknowledges the National Science Foundation for support under Grant No. CHE-1213771. The computing for this project was performed on the Beocat Research Cluster at Kansas State University, which is funded in part by NSF Grants CNS-1006860, EPS-1006860, and EPS-0919443. We thank Ilia A. Guzei for single-crystal X-ray measurement and analysis; Henry Valle for help with crystal screening; and Rangana Warshamanage for guidance on initial crystallization setups and the reviewers for helping to improve the presentation of the manuscript.

■ REFERENCES

(1) Devadas, M. S.; Bairu, S.; Qian, H.; Sinn, E.; Jin, R.; Ramakrishna, G. Temperature-Dependent Optical Absorption Properties of Monolayer-Protected Au_{25} and Au_{38} Clusters. *J. Phys. Chem. Lett.* **2011**, *2*, 2752−2758.

(2) Antonello, S.; Perera, N. V; Ruzzi, M.; Gasco, J. A.; Maran, F. Interplay of Charge State, Lability, and Magetism in the Molecule-Like $Au_{25}(SR)_{18}$. *J. Am. Chem. Soc.* **2013**, *135*, 15585−15594.

(3) Negishi, Y.; Iwai, T.; Ide, M. Continuous Modulation of Electronic Structure of Stable Thiolate-Protected Au_{25} Cluster by Ag Doping. *Chem. Commun.* **2010**, *46*, 4713−4715.

(4) Negishi, Y.; Kurashige, W.; Niihori, Y.; Iwasa, T.; Nobusada, K. Isolation, Structure, And Stability of a Dodecanethiolate-Protected Pd_1Au_{24} Cluster. *Phys. Chem. Chem. Phys.* **2010**, *12*, 6219−6225.

(5) Negishi, Y.; Munakata, K.; Ohgake, W.; Nobusada, K. Effect of Copper Doping on Electronic Structure, Geometric Structure, and Stability of Thiolate-Protected Au_{25} Nanoclusters. *J. Phys. Chem. Lett.* **2012**, *3*, 2209−2214.

(6) Qian, H.; Jiang, D.-e.; Li, G.; Gayathri, C.; Das, A.; Gil, R. R.; Jin, R. Monoplatinum Doping of Gold Nanoclusters and Catalytic Application. *J. Am. Chem. Soc.* **2012**, *134*, 16159−16162.

(7) Schwerdtfeger, P. Gold Goes Nano—From Small Clusters to Low-Dimensional Assemblies. *Angew. Chem. Int. Ed.* **2003**, *42*, 1892−1895.

(8) Walter, M.; Moseler, M. Ligand-Protected Gold Alloy Clusters: Doping the Superatom. *J. Phys. Chem. C* **2009**, *113*, 15834−15837.

(9) Guidez, E. B.; Mäkinen, V.; Häkkinen, H.; Aikens, C. M. Effects of Silver Doping on the Geometric and Electronic Structure and Optical Absorption Spectra of the $Au_{25-n}Ag_n(SH)_{18}^-$ (n = 1, 2, 4, 6, 8, 10, 12) Bimetallic Nanoclusters. *J. Phys. Chem. C* **2012**, *116*, 20617−20624.

(10) Kauffman, D. R.; Alfonso, D.; Matranga, C.; Qian, H.; Jin, R. A Quantum Alloy: The Ligand-Protected $Au_{25-x}Ag_x(SR)_{18}$ Cluster. *J. Phys. Chem. C* **2013**, *117*, 7914−7923.

(11) Kumara, C.; Dass, A. AuAg Alloy Nanomolecules with 38 Metal Atoms. *Nanoscale* **2012**, *4*, 4084−4086.

(12) Kumara, C.; Dass, A. $(AuAg)_{144}(SR)_{60}$ Alloy Nanomolecules. *Nanoscale* **2011**, *3*, 3064−3067.

(13) Mednikov, E. G.; Jewell, M. C.; Dahl, L. F. Nanosized (μ_{12}-Pt)$Pd_{164-x}Pt_x(CO)_{72}(PPh_3)_{20}$ ($x \approx 7$) Containing Pt-Centered Four-Shell 165-Atom Pd−Pt Core with Unprecedented Intershell Bridging Carbonyl Ligands: Comparative Analysis of Icosahedral Shell-Growth Patterns with Geometrically Related $Pd_{145}(CO)_x(PEt_3)_{30}$ ($x \approx 60$) Containing Capped Three-Shell Pd_{145} Core. *J. Am. Chem. Soc.* **2007**, *129*, 11619−11630.

(14) Mednikov, E. G.; Ivanov, S. A.; Dahl, L. F. CO-Induced Formation of an Interpenetrating Bicuboctahedral Au_2Pd_{18} Kernel in Nanosized $Au_2Pd_{28}(CO)_{26}(PEt_3)_{10}$: Formal Replacement of an Interior $(\mu_{12}$-Pd$)_2$ Fragment in the Corresponding Known Isostructural Homopalladium $Pd_{30}(CO)_{26}(PEt_3)_{10}$ with Nonisovalent (μ_{12}-Au$)_2$ and Resulting Experimental/Theoretical Implications. *Inorg. Chem.* **2011**, *50*, 11795−11806.

(15) Malola, S.; Häkkinen, H. Electronic Structure and Bonding of Icosahedral Core−Shell Gold−Silver Nanoalloy Clusters $Au_{144-x}Ag_x(SR)_{60}$. *J. Phys. Chem. Lett* **2011**, *2*, 2316−2321.

(16) Heaven, M. W.; Dass, A.; White, P. S.; Holt, K. M.; Murray, R. W. Crystal Structure of the Gold Nanoparticle $[N(C_8H_{17})_4]$-$[Au_{25}(SCH_2CH_2Ph)_{18}]$. *J. Am. Chem. Soc.* **2008**, *130*, 3754−3755.

(17) Zhu, M.; Aikens, C. M.; Hollander, F. J.; Schatz, G. C.; Jin, R. Correlating the Crystal Structure of A Thiol-Protected Au_{25} Cluster and Optical Properties. *J. Am. Chem. Soc.* **2008**, *130*, 5883−5885.

(18) Desireddy, A.; Conn, B. E.; Guo, J.; Yoon, B.; Barnett, R. N.; Monahan, B. M.; Kirschbaum, K.; Griffith, W. P.; Whetten, R. L.; Landman, U.; Bigioni, T. P. Ultrastable Silver Nanoparticles. *Nature* **2013**, *501*, 399−402.

(19) Yang, H.; Wang, Y.; Huang, H.; Gell, L.; Lehtovaara, L.; Malola, S.; Häkkinen, H.; Zheng, N. All-Thiol-Stabilized Ag_{44} and $Au_{12}Ag_{32}$ Nanoparticles with Single-Crystal Structures. *Nat. Commun.* **2013**, *4*, 2422.

(20) The fraction of each of the $Au_{25-x}Ag_x(SR)_{18}$ nanomolecule, where x = 4, 5, 6, 7, and 8, was calculated from the peak height corresponding to each species. That is, each fraction was obtained using the following formula: fraction of $Au_{19}Ag_6(SR)_{18}$ = (peak height of $Au_{19}Ag_6(SR)_{18}$/sum of all peaks corresponding to x = 4, 5, 6, 7 and 8) = 95.66/226.02 = 0.423.

(21) Aikens, C. M. Origin of Discrete Optical Absorption Spectra of $M_{25}(SH)_{18}^-$ Nanoparticles (M = Au, Ag). *J. Phys. Chem. C* **2008**, *112*, 19797−19800.

(22) van Leeuwen, R.; Baerends, E. J. Exchange−Correlation Potential with Correct Asymptotic Behavior. *Phys. Rev. A* **1994**, *49*, 2421−2431.

(23) van Lenthe, E.; Baerends, E. J.; Snijders, J. G. Relativistic Total Energy Using Regular Approximations. *J. Chem. Phys.* **1994**, *101*, 9783−9792.

(24) te Velde, G.; Bickelhaupt, F. M.; Baerends, E. J.; Fonseca Guerra, C.; van Gisbergen, S. J. A.; Snijders, J. G.; Ziegler, T. Chemistry with ADF. *J. Comput. Chem.* **2001**, *22*, 931−967.